DALTON
FULL PAPER

Spatial distribution of valence electrons in metallocenes studied by Penning ionization electron spectroscopy

Hideki Mutoh and Shigeru Masuda

Department of Chemistry, Graduate School of Arts and Sciences, The University of Tokyo, Komaba, Meguro, Tokyo 153-8902, Japan. E-mail: masuda@piesap.c.u-tokyo.ac.jp

Received 17th December 2001, Accepted 21st February 2002
First published as an Advance Article on the web 11th April 2002

Penning ionization electron spectra resulting from thermal collisions of He*(1s2s, 2^3S) metastable atoms with gaseous metallocenes, $M(C_5H_5)_2$ (M = V, Cr, Mn, Fe, Co, Ni, Ru, and Os), were measured to directly probe the spatial electron distribution of the metal d-derived orbitals. Owing to the strong antibonding d–π interactions the metallic e_1'' orbitals in $Mn(C_5H_5)_2$, $Ni(C_5H_5)_2$, and especially $Co(C_5H_5)_2$, show rather diffuse electron distributions. In contrast, the Cp π-derived e_1'' orbitals exhibit compact distributions due to the bonding d–π interactions, which is clearly seen in the cases of $Ru(C_5H_5)_2$ and $Os(C_5H_5)_2$. For the metallic e_2' and a_1' orbitals with essentially nonbonding character, the radial extent of the d orbitals increase on going from $Fe(C_5H_5)_2$ to $Ru(C_5H_5)_2$ and $Os(C_5H_5)_2$, as expected. $Mn(C_5H_5)_2$ is anomalous among the 3d metallocenes, because the nonbonding e_2' and a_1' orbitals are significantly contracted in space, reflecting their highly ionic character.

Introduction

Over recent years the electronic properties of bis(cyclopentadienyl) compounds have attracted considerable attention from both experimental and theoretical viewpoints.[1] In particular, metallocenes involving a metal atom in the first transition series have been regarded as prototypes for understanding the metal–ligand interactions in ordinary organometallic compounds because they have a simple sandwich structure belonging to the D_{5d} or D_{5h} point group.[2] Furthermore, the 3d metallocenes show various spin states; ferrocene is a closed-shell (diamagnetic) molecule with d^6 configuration while the other 3d metallocenes are open-shell (paramagnetic) molecules. These features provide a model system for verifying the validity (or limitations) of the ligand field theory and several molecular orbital calculations, through the multiplet splittings of the d-derived states, the level ordering of the ground and the ionic states, *etc*.

The nature of the chemical bond in a metallocene molecule, MCp_2, has been described in terms of d–π interactions.[3] Fig. 1

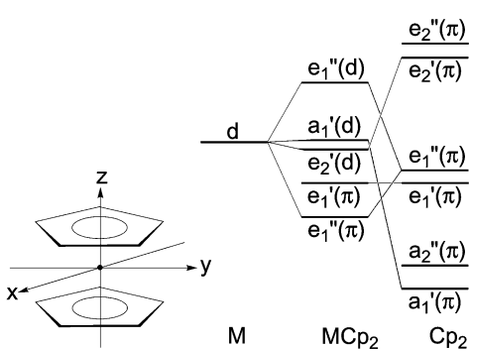

Fig. 1 Schematic energy diagram of a metallocene molecule.

shows a schematic energy diagram for a metallocene. In the D_{5h} ligand field, the metal d states split into three levels; d_{xy} and $d_{x^2-y^2}$ orbitals mix with an empty Cp π orbital to form an e_2' MO, the d_{z^2} orbital couples with a lower-lying occupied Cp π orbital to form an a_1' MO, and d_{yz} and d_{zx} orbitals hybridize strongly with higher-lying occupied Cp π orbitals to form an antibonding e_1'' MO. Owing to the large energy gaps and small wavefunction overlap between the d and π states, the former two interactions are so weak that the e_2' and especially a_1' MOs can be regarded as essentially nonbonding orbitals. Thus, the metal d-derived states are arranged in the order $e_1'' > a_1' > e_2'$. As for the Cp π-derived states, the e_1'' MO is a bonding type including the metal d_{yz} and d_{zx} components and the e_1' MO is a nonbonding type without any metal d contributions. As a consequence, the ground state configuration of the metallocene is expressed in the form, $e_1''(\pi)^4e_1'(\pi)^4e_2'(d)^xa_1'(d)^ye_1''(d)^z$. Table 1 shows the electronic configurations in the ground and ionic states of the metallocene molecules in the present study.

The ultraviolet photoelectron spectra (UPS) of metallocenes have been measured several times;[4–7] with the following characteristics: (1) The lowest ionic state of $Fe(C_5H_5)_2$ is $^2E_2'$, which means that the Koopmans' theorem breaks down, owing to the strong relaxation effect upon d ionization.[8,9] (2) In the case of the open-shell derivatives, the d-derived multiplet structures can be interpreted well on the basis of the ligand field theory.[10] A better agreement is obtained when the configuration interaction is taken into account.[7] (3) The ground state of $Cr(C_5H_5)_2$ is $^3E_2'$ rather than $^3A_2'$.[6] $Mn(C_5H_5)_2$ is a high-spin complex at least in the gas phase, while $Mn(C_5Me_5)_2$ is a low-spin complex.[7] (4) The level orderings of the ionic states of $V(C_5H_5)_2$, $Mn(C_5H_5)_2$, and $Fe(C_5H_5)_2$ are now fairly well established, while those for $Cr(C_5H_5)_2$, $Co(C_5H_5)_2$, and $Ni(C_5H_5)_2$ are incomplete.

In addition to the level orderings and spin states, the spatial electron distributions of the d-derived orbitals would be a key factor for understanding metal–ligand interactions, chemical reactivities with other molecules, electronic and magnetic properties in the condensed phase, *etc.*, but the experimental information remains rather limited.

In the present study, we shed light on the spatial extent of the d-derived orbitals of metallocenes, $M(C_5H_5)_2$ (M = V, Cr, Mn, Fe, Co, Ni, Ru, and Os), by utilizing Penning ionization electron spectroscopy. This method is based on the energy analysis of electrons emitted by thermal collisions between a rare-gas metastable atom such as He*(2^3S) and a target molecule (T):

$$T + He^*(1s2s, 2^3S) \longrightarrow T^+ + He(1s^2, 1^1S) + e^-$$

DOI: 10.1039/b111486g

Table 1 Electron configurations of the d-derived states for metallocenes in the present study

Compound	Ground state configuration	Orbital ionization	Ionic state
$V(C_5H_5)_2$	$^4A_2'$, $(e_2')^2(a_1')^1$	e_2'	$^3E_2'$
		a_1'	$^3A_2'$
$Cr(C_5H_5)_2$	$^3E_2'$, $(e_2')^3(a_1')^1$	e_2'	$^4A_2' + {}^2A_2' + {}^2A_1' + {}^2E_1''$
		a_1'	$^2E_2'$
$Mn(C_5H_5)_2$	$^6A_1'$, $(e_2')^2(a_1')^1(e_1'')^2$	e_2'	$^5E_2'$
		a_1'	$^5A_1'$
		e_1''	$^5E_1''$
$Fe(C_5H_5)_2$, $Ru(C_5H_5)_2$, $Os(C_5H_5)_2$	$^1A_1'$, $(e_2')^4(a_1')^2$	e_2'	$^2E_2'$
		a_1'	$^2A_1'$
$Co(C_5H_5)_2$	$^2E_1''$, $(e_2')^4(a_1')^2(e_1'')^1$	e_2'	$^3E_1'' + {}^1E_1'' + {}^3E_2' + {}^1E_2'$
		a_1'	$^3E_1'' + {}^1E_1''$
		e_1''	$^1A_1'$
$Ni(C_5H_5)_2$	$^3A_2'$, $(e_2')^4(a_1')^2(e_1'')^2$	e_2'	$^4E_2' + {}^2E_2'$
		a_1'	$^4A_2' + {}^2A_2'$
		e_1''	$^2E_1''$

In the process, a valence electron of T fills the 1s hole of He*(2^3S) and the 2s electron is emitted to a continuum state, simultaneously.[11] Since the transition probability for the electron transfer largely depends on the spatial overlap between the occupied orbital of T and the empty 1s orbital of He*, an orbital exposed outside the repulsive molecular surface interacts more effectively with He* than does an orbital localized inside the molecule, yielding a stronger band in the spectrum.[12] Since the pioneering work on the Ne*–$Fe(C_5H_5)_2$ collision system by Munakata *et al.*,[13] this simple feature of Penning ionization has been applied to probe the spatial electron distribution in organometallic compounds such as $M(CH_3)_4$ (M = C, Si, Ge, Sn),[14] $Fe(CO)_5$,[15] $M(CO)_6$ (M = Cr, Mo, W),[16] $Fe(C_5H_5)_2$ and $Cr(C_6H_6)_2$,[17] $Co(C_5H_5)_2$,[18] *etc*.

Experimental

The details of the experimental apparatus and related procedures used have been described in previous reports.[15,16] The ionization chamber was newly constructed for the present study to reduce the amount of sample necessary for the measurement. The He* metastable atoms [2^1S (20.62 eV) and 2^3S (19.82 eV)] were produced by cold discharge. A glass helium discharge lamp was used to quench 2^1S atoms and a pure 2^3S atom beam was obtained for Penning ionization electron spectra. The He I resonance line (21.22 eV) was used for ultraviolet photoelectron spectra. The spectra were measured by a 180° hemispherical-type analyzer with an energy resolution of about 30 meV. The detection angle of emitted electrons was 90° with respect to the He* and the photon beams. The relative band intensity of the spectra was calibrated by a transmission efficiency curve of the spectrometer. High-purity samples were obtained commercially and used without further purification. The samples were heated to 30~80 °C in the ionization chamber to obtain sufficient sample pressure.

Results and discussion

Fig. 2 shows the He I ultraviolet photoelectron spectra (UPS) and He*(2^3S) Penning ionization electron spectra (PIES) of gaseous metallocenes, $M(C_5H_5)_2$ (M = V, Cr, Mn, Fe, Co, Ni, Ru, and Os). For the sake of comparison between the UPS and PIES, the energy scales for the PIES are shifted to those for the UPS by the difference in the excitation energy, 21.22 − 19.82 = 1.40 eV.

Assignment of UPS and PIES bands

$Fe(C_5H_5)_2$, $Ru(C_5H_5)_2$, and $Os(C_5H_5)_2$ are closed-shell molecules with an electron configuration of $e_2'(d)^4a_1'(d)^2$, $^1A_1'$. The photoelectron spectrum of $Fe(C_5H_5)_2$ has been measured several times and the assignment is now well-established; the first two bands, 1 and 2, are attributed to electron emission from the Fe 3d-derived e_2' and a_1' states leading to the $^2E_2'$ and $^2A_1'$ ionic states, whereas the next two bands, 3 and 4, are those from the Cp π-derived e_1' and e_1'' states.[4–7] The corresponding bands also appear in the PIES and can be attributed to the same origins. As seen in Fig. 2, however, the relative band intensity differs considerably between the two spectra. For example, the metallic e_2'-derived band is about two times stronger than the a_1'-derived band in the UPS reflecting the orbital degeneracy, while the two metallic bands show a similar intensity in the PIES. The latter feature is based on the mechanism of Penning ionization (see next section for details) and serves as a useful guide for assignment of photoelectron bands.

As for the UPS of $Ru(C_5H_5)_2$, band 1 has been assigned to the nearly-degenerate Ru 4d-derived a_1' and e_2' states, while bands 2 and 3 are due to the Cp π-derived e_1' and e_1'' states, respectively.[5,7] In the case of $Os(C_5H_5)_2$, the first three photoelectron bands show a similar intensity and can be attributed to the Os 5d-derived e_2' and a_1' states by analogy with the assignment for $Os(C_5H_4CH_3)_2$;[5] bands 1 and 3 are produced by spin–orbit coupling for the orbitally degenerate $^2E_2'$ ionic states, $^2E_2'(5/2)$ and $^2E_2'(3/2)$, and band 2 is assigned to the $^2A_1'$ ionic state. This assignment is further confirmed by the PIES, where the a_1'-derived band 2 is much stronger than the e_2'-derived bands 1 and 3, as in the case of $Fe(C_5H_5)_2$. Bands 4 and 5 are assigned to the Cp π-derived e_1' and e_1'' states, respectively.

$V(C_5H_5)_2$ is an open-shell molecule with the high-spin configuration of $e_2'(d)^2a_1'(d)^1$, $^4A_2'$. The electron emission from the V 3d-derived e_2' and a_1' states give rise to two triplet states, $^3E_2'$ and $^3A_2'$, respectively. In the UPS, only a single band observed in the IE = 6–8 eV region is assigned to the two d-derived states and the next band, 2, to the Cp π-derived e_1' and e_1'' states.[6,7]

$Cr(C_5H_5)_2$ has the ground-state configuration of $e_2'(d)^3a_1'(d)^1$, $^3E_2'$. The electron emission from the e_2' state leads to the $^4A_2'$, $^2A_2'$, $^2A_1'$, and $^2E_1''$ ionic states, and that from the a_1' state to the $^2E_2'$ ionic state. The He I spectrum shows four bands, 1–4, in the IE = 5–8 eV region, but the detailed assignment is unclear. Rabalais *et al.* examined the branching ratio of the d-derived states on the basis of the ligand field theory and assigned bands 1–4 to the $^2E_2'$, $^4A_2'$, $^2E_1''$, and $^2A_1' + {}^2A_2'$ states.[4] Evans *et al.* analyzed the intensity ratio in more detail and suggested that bands 1–4 can possibly be assigned to the $^4A_2'$, $^2E_1''$, $^2A_1'$, and $^2A_2'$ states or the $^4A_2'$, $^2E_1'' + {}^2E_2'$, $^2A_1'$, and $^2A_2'$ states.[6] Cauletti *et al.*, on the other hand, compared the He I and He II spectra and assigned bands 1–4 to the $^4A_2'$, $^2E_1''$, $^2E_2'$, and $^2A_1' + {}^2A_2'$ states.[7] If we assign the first band to the quartet state from the energetic point of view, the remaining bands 2–4 should be due to the doublet states. As is seen in the PIES, band 3 is stronger than bands 2 and 4, and therefore it can possibly be attributed to emission from the a_1' state ($^2E_2'$ ionic state), as in the case of $Fe(C_5H_5)_2$, which favors the assignment by Cauletti

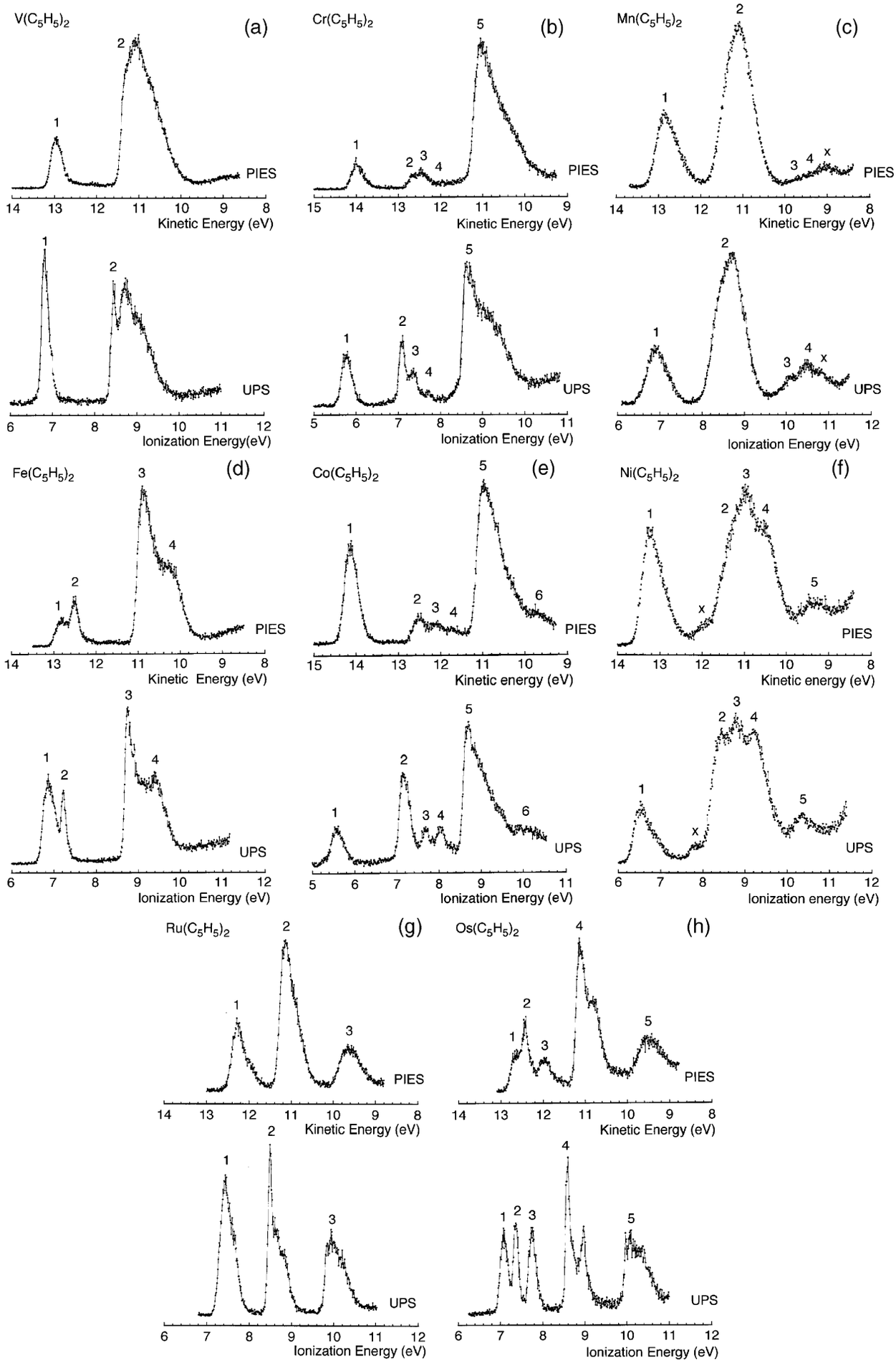

Fig. 2 He I UPS and He*(2^3S) PIES of metallocene molecules, $M(C_5H_5)_2$ (M = V, Cr, Mn, Fe, Co, Ni, Ru, and Os).

et al. The photoelectron band 5 is commonly assigned to emission from the Cp π-derived e_1' and e_1'' states.

$Mn(C_5H_5)_2$ is a high-spin compound with the ground-state configuration of $e_2'(d)^2a_1'(d)^1e_1''(d)^2$, $^6A_1'$. The electron emission from the e_2', a_1', and e_1'' states yields the $^5E_2'$, $^5A_1'$, and $^5E_1''$ ionic states, respectively. The photoelectron bands 1, 3, and 4 are assigned to the $^5E_1''$, $^5A_1'$, and $^5E_2'$ states, while band 2 is assigned to Cp π-derived e_1' and e_1'' states.[4,6,7] Band X is due to cyclopentadiene impurity.[4]

$Co(C_5H_5)_2$ has the ground-state configuration of $e_2'(d)^4a_1'(d)^2e_1''(d)^1$, $^2E_1''$. The electron emission from the e_2' state leads to the $^3E_1''$, $^1E_1''$, $^3E_2'$, and $^1E_2'$ ionic states, that from the a_1' state to the $^3E_1''$ and $^1E_1''$ ionic states, and that from the e_1'' state to the $^1A_1'$ ionic state. The He I spectrum shows six bands, 1–6, in the IE = 5–10.5 eV region, but the complete assignment has not been made; band 1 has been attributed to the e_1''-derived $^1A_1'$ ionic state, and bands 2–4 and 6 to the e_2'- and a_1'-derived ionic states.[6,7] Band 5 is attributed to the Cp π-derived states.

$Ni(C_5H_5)_2$ has the ground-state configuration of $e_2'(d)^4a_1'(d)^2e_1''(d)^2$, $^3A_2'$. The electron emission from the e_2' state gives rise to the $^4E_2'$ and $^2E_2'$ ionic states, that from the a_1' state to the $^4A_2'$ and $^2A_2'$ ionic states, and that from the e_1'' state to the $^2E_1''$ ionic state. The He I spectrum shows five bands, 1–5, in the IE = 6–11 eV region. Since the ionic states formed upon d ionization overlap with those resulting from Cp π ionization, the complete assignment is difficult, as in the case of $Co(C_5H_5)_2$. Evans *et al.* and Cauletti *et al.* indicated that the lowest IE band, 1, is assigned to the e_1''-derived $^2E_1''$ ionic state, bands 2 and 4 to the e_2'- and a_1'-derived ionic states, and band 3 to the Cp π-derived states.[6,7]

Fig. 3 shows a change in the ionization energy of the d-derived states across the 3d metallocenes. The e_2'- and a_1'-

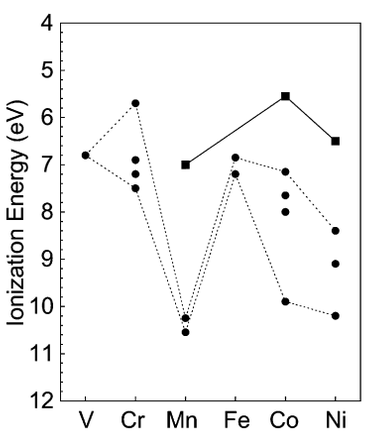

Fig. 3 Ionization energy of metallocene molecules, $M(C_5H_5)_2$ (M = V, Cr, Mn, Fe, Co, Ni, Ru, and Os).

derived states denoted by circles are distributed over a wide energy range (1.8–2.8 eV) in the cases of $Cr(C_5H_5)_2$, $Co(C_5H_5)_2$, and $Ni(C_5H_5)_2$ reflecting the rich multiplet structures, while the energy separations are rather small (≤0.35 eV) for $V(C_5H_5)_2$, $Mn(C_5H_5)_2$, and $Fe(C_5H_5)_2$. The averaged ionization energy of these metallic states are slightly changed in the lighter (V–Fe) metallocenes, except for $Mn(C_5H_5)_2$, and then shifted to lower values on going from $Fe(C_5H_5)_2$ to $Co(C_5H_5)_2$ and $Ni(C_5H_5)_2$. The e_1''-derived states denoted by squares in Fig. 3 are seen in the cases of $Mn(C_5H_5)_2$, $Co(C_5H_5)_2$, and $Ni(C_5H_5)_2$. These features are in agreement with previous UPS studies.[6,7]

In the thermal collision of the He*(2^3S) atom with an open-shell molecule (T) such as O_2, it is known that the ionic decay channel operates as a competing process of Penning ionization.[19] The ionic channel is composed of a two-step process;

$$T + He^*(1s2s, 2^3S) \longrightarrow T^- + He^+(1s, 1^2S) \longrightarrow T^+ + He(1s^2, 1^1S) + e^-$$

where the 2s electron of He*(2^3S) transfers to an empty orbital of T (ion pair formation), and then a valence electron of T^- fills the 1s hole of He^+ and another valence electron of T^- is simultaneously emitted to a continuum state (autoionization). Owing to the Coulomb interaction in the intermediate state, this decay channel gives rise to a broad and rather featureless structure in the spectrum. As is seen in Fig. 2, however, all the bands in the PIES of the metallocene molecules correspond well to the photoelectron bands and show little background, at least in the ionization energy region above 11 eV. This indicates that the He*(2^3S) atoms deexcite predominantly *via* Penning ionization for open-shell metallocenes as in the cases for closed-shell metallocenes.

Spatial electron distribution of the d-derived orbitals

Before a detailed analysis of the PIES shown in Fig. 2, we should mention the collision geometry between the He*(2^3S) atoms and the metallocene molecules. Fig. 4(a) shows a

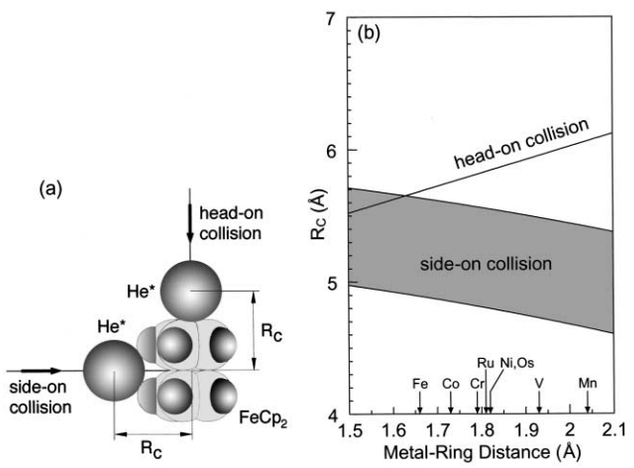

Fig. 4 (a) Collision geometry in the He*(2^3S)–$Fe(C_5H_5)_2$ system based on the hard collision model. (b) Relation between the classical turning points, R_C, and the metal–ring distances, d_{M-Cp}, in the metallocenes (see text).

schematic view of the He*(2^3S)–$Fe(C_5H_5)_2$ collision system on the basis of the hard collision model, in which $Fe(C_5H_5)_2$ and He*(2^3S) are represented by the van der Waals spheres of the constituent H and C atoms (r_H = 1.20 Å and r_C = 1.70 Å) and the effective radius of He*(2^3S) (r_{He^*} = 2.5 Å).[20] In the head-on collision where the He*(2^3S) atom approaches the Fe atom in $Fe(C_5H_5)_2$ in the direction of the five-fold symmetry axis, the classical turning point, R_C, is 5.68 Å when the metal-to-ring distance (d_{M-Cp}) is taken to be 1.66 Å.[2] In the side-on collision where the metastable atom accesses the Fe atom in $Fe(C_5H_5)_2$ in the horizontal mirror plane, R_C depends on the azimuth and ranges to 4.89–5.64 Å. The hard collision model may be oversimplified for describing the actual Penning ionization, because R_C is known to be affected by the collision energy and the shape of the potential energy surface between the He*(2^3S) atom and a target molecule.[18,21] It is evident, however, that the He*(2^3S) atom can not impinge directly on the metal atom in $Fe(C_5H_5)_2$ in any collision geometry, since the ion radius of Fe^{2+} is only 0.75 Å. Fig. 4(b) shows the relation between R_C and d_{M-Cp} in the He*(2^3S) collision with metallocences. With increasing d_{M-Cp}, R_C is lengthened linearly in the head-on collision, whereas it is shortened almost linearly in the side-on collision. As mentioned in the Introduction, Penning ionization occurs through spatial overlap between the 1s orbital of He*(2^3S) and a relevant molecular orbital of the metallocene, so that the ionization rates for the metal d-derived orbitals increase exponentially with decreasing R_C. In this sense, the metal–ring distance (which determines R_C) is an important factor for Penning ioniz-

ation of metallocene molecules as well as the spatial electron distribution of the d-derived orbitals.

First we deal with the Penning ionization from the metallic e_2' (primarily d_{xy} and $d_{x^2-y^2}$) and a_1' (essentially d_{z^2}) orbitals on the basis of the radial and angular distributions. Fig. 5 shows

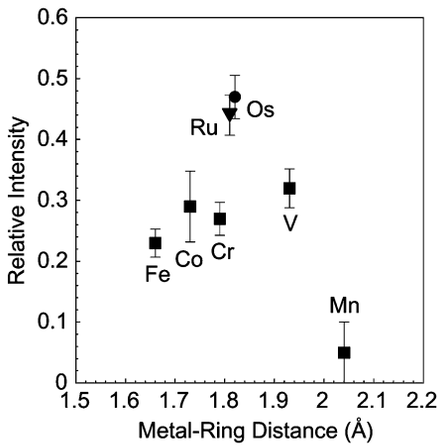

Fig. 5 Relative intensity of the metallic e_2'- and a_1'-derived bands in the PIES of metallocene molecules (see text).

the relative intensity of the metallic bands in the PIES as a function of the metal–ring distance, d_{M-Cp}. To facilitate comparison among the compounds, it was obtained relative to the intensity of the Cp π-derived bands and then normalized by the number of electrons, 8 and N, in the Cp π and metallic orbitals, *i.e.*, $(8/N) \times [I(e_2') + I(a_1')]/[I(Cp\ \pi)]$. Here the data for $Ni(C_5H_5)_2$ are not shown owing to the heavy band overlap. As a common feature of the metallocenes, the Penning ionization rates for the metal d-derived e_2' and a_1' orbitals are significantly suppressed compared with those for the Cp π-derived orbitals. This indicates that the metallic orbitals are localized well inside the molecule owing to their nonbonding character and cannot overlap effectively with the 1s state of the incident $He^*(2^3S)$ atom, as reported first in the Ne^*–$Fe(C_5H_5)_2$ collision system.[13] It is noted that such a marked suppression is not seen in the Penning spectra of formally zero-valent sandwich compounds like dibenzenechromium, $Cr(C_6H_6)_2$, where the a_{1g} orbital (corresponding to the a_1' orbital in metallocene) shows a comparable ionization rate to the benzene π-derived orbitals.[17] The characteristics of the PIES of metallocenes found here are summarized as follows: (1) It is clear from Fig. 5 that the Penning ionization rates for the metallic e_2' and a_1' orbitals increase steeply on going from $Fe(C_5H_5)_2$ to $Ru(C_5H_5)_2$ and $Os(C_5H_5)_2$. A part of this increase is undoubtedly due to the enlargement of the radial size of the metal d orbitals from 3d to 4d and 5d. The slight change in the latter two compounds corresponds well to the fact that the Os 5d orbitals are contracted to sizes similar to the Ru 4d orbitals owing to so-called lanthanide contraction. Actually the metal-to-ring distance in $Os(C_5H_5)_2$ (d_{M-Cp} = 1.82 Å)[22] is almost the same as that in $Ru(C_5H_5)_2$ (d_{M-Cp} = 1.81 Å).[23] The increase in the radial extent of the d orbitals in the series, $Fe(C_5H_5)_2 \ll Ru(C_5H_5)_2 \leqslant Os(C_5H_5)_2$, is consistent with the trend with respect to the ability of these molecules to serve as electron donors in metal–hydrogen bonds.[24,25] (2) In the 3d series, the Penning ionization probabilities for the metallic orbitals rise gradually in the order $Fe(C_5H_5)_2$, $Co(C_5H_5)_2$, $Cr(C_5H_5)_2$, and $V(C_5H_5)_2$. This tendency shows a good correlation to the elongation of the metal–ring distance d_{M-Cp}. As shown in Fig. 4(b), when the metal–ring distance is lengthened, the $He^*(2^3S)$ atom approaches more closely the metal atom especially in the side-on collision, yielding an increased emission from the metallic states (see below for details). (3) In Fig. 5 $Mn(C_5H_5)_2$ is anomalous. The metallic e_2'- and a_1'-derived bands are barely present in the Penning spectrum, although it has a longer metal–ring distance (d_{M-Cp} = 2.04 Å)[2] compared with the other 3d metallocenes. This inactive feature for Penning ionization provides direct evidence that the Mn 3d orbitals are heavily contracted owing to the highly ionic character of Mn in $Mn(C_5H_5)_2$. Due to the less screened nuclear charge thus formed, the e_2'- and a_1'-derived states in $Mn(C_5H_5)_2$ are shifted to the higher ionization energy side relative to those in the other 3d metallocenes (see Fig. 3). Our data may explain the chemical reactivity of $Mn(C_5H_5)_2$;[26,27] for example, it reacts easily with iron(II) chloride in tetrahydrofuran to give $Fe(C_5H_5)_2$.

In the cases of $Cr(C_5H_5)_2$, $Fe(C_5H_5)_2$, and $Os(C_5H_5)_2$, the metallic e_2'- and a_1'-derived bands are separated fairly well in the PIES. As mentioned above, the PIES of $Fe(C_5H_5)_2$ show that the a_1'-derived band is much more intense relative to the e_2'-derived band, taking the number of occupied electrons into account. The normalized intensity ratio, $4/2 \times I(a_1')/I(e_2')$, is 2.2 ± 0.2. With increasing metal-to-ring distance, the corresponding ratios are decreased to 1.3 ± 0.3 for $Cr(C_5H_5)_2$ and 1.4 ± 0.2 for $Os(C_5H_5)_2$. These features indicate that the Penning ionization from the a_1' and e_2' orbitals originates mainly when the $He^*(2^3S)$ atom approaches normal and parallel to the Cp rings, respectively. As is shown in Fig. 4(b), R_C in the normal approach is lengthened by an extension of the metal–ring distance to yield a smaller overlap between the $He^*(2^3S)$ 1s orbital and the metallic orbitals, while R_C in the parallel approach is shortened to yield a larger overlap. In other words, our data really show that the metallic a_1' orbital extends normal to the Cp rings and the metallic e_2' orbital is distributed parallel to the Cp rings, as expected. The enhancement of the a_1'-derived band over the e_2'-derived band in $Fe(C_5H_5)_2$ suggests that the $3d_{z^2}$ orbital extends further outside the molecule than the cases of $3d_{xy}$ and $3d_{x^2-y^2}$ orbitals, reflecting the difference in the angular distributions.

Next we will shed light on the spatial extent of the bonding and antibonding e_1'' orbitals, *i.e.*, $e_1''(\pi)$ and $e_1''(d)$. Fig. 6 shows

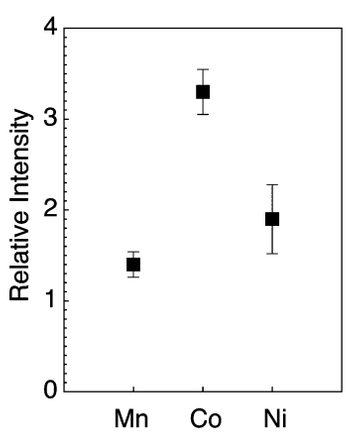

Fig. 6 Relative intensity of the metallic e_1''-derived bands in the PIES of $Mn(C_5H_5)_2$, $Co(C_5H_5)_2$, and $Ni(C_5H_5)_2$ molecules (see text).

the relative intensity of the $e_1''(d)$-derived bands in the PIES of $Mn(C_5H_5)_2$, $Co(C_5H_5)_2$, and $Ni(C_5H_5)_2$. For a comparison among the compounds, it was estimated with respect to the intensity of the Cp π-derived bands and normalized by the number of electrons in the Cp π and d orbitals, *i.e.*, $(8/N) \times [I(d)]/[I(Cp\ \pi)]$. As seen in Fig. 6 and the relevant spectra, the Penning ionization rates for the $e_1''(d)$ orbital are surprisingly higher than those for the $e_2'(d)$ and $a_1'(d)$ orbitals. The enhancement clearly shows that the $e_1''(d)$ orbital has a rather diffuse electron distribution owing to the strong d–π coupling. This feature is in good agreement with theoretical results, including Xα calculations for $Fe(C_5H_5)_2$,[28,29] $Co(C_5H_5)_2$,[30,31] $Ni(C_5H_5)_2$,[32] $Ru(C_5H_5)_2$,[33] and *ab initio* SCF calculations for $Fe(C_5H_5)_2$.[8,9] However, we should emphasize here that the

wavefunction tails of the e_1''(d) orbital extend further outside the molecule even when compared with those of the pure Cp π orbitals. This finding may be simply interpreted as described below.

Within the molecular orbital scheme, the bonding and antibonding e_1'' orbitals, ψ_B and ψ_A, may be expressed by:

$$\psi_B = (b_1^2 + 2b_1b_2S + b_2^2)^{-1/2}(b_1\psi_d + b_2\psi_\pi)\ (b_1, b_2 > 0) \quad (1)$$

$$\psi_A = (a_1^2 - 2a_1a_2S + a_2^2)^{-1/2}(a_1\psi_d - a_2\psi_\pi)\ (a_1, a_2 > 0) \quad (2)$$

where S denotes the overlap integral between the metal d and Cp π orbitals. In the bonding orbital, the d–π mixing occurs in-phase and therefore the wavefunction tails shrink in the region outside the Cp rings compared to the original π orbital. In the antibonding orbital the d–π coupling takes place out-of-phase. If the mixing ratio (a_2/a_1) is larger than 2S, the wavefunction tails would extend farther away from the Cp rings than those of the pure π orbital. In other words, the antibonding d–π interaction in metallocene squeezes Cp π electrons from the bonding region to the outside of the Cp rings, to form a diffuse electron distribution.

In Fig. 6 the Penning ionization rate for the e_1''(d) orbital increases when going from $Mn(C_5H_5)_2$ to $Ni(C_5H_5)_2$ and $Co(C_5H_5)_2$. This sequence can possibly be interpreted in terms of the strength of the antibonding d–π interactions in the metallocenes. When the metal–ring bonding is weakened by electron occupancy in the antibonding state, the metal–ring distances are lengthened on going from singly-occupied $Co(C_5H_5)_2$ (1.73 Å) to doubly-occupied $Ni(C_5H_5)_2$ (1.82 Å) and $Mn(C_5H_5)_2$ (2.04 Å).[2] As a result of the extension, the overlap between the metal d and Cp π orbitals is decreased, and the wavefunction tail of the e_1''(d) state is less exposed outside the molecule. Our interpretation is consistent with the sequence of the ionization energy of the e_1''(d)-derived states shown in Fig. 3, where the e_1''(d) state of $Co(C_5H_5)_2$ is destabilized significantly compared with those of $Ni(C_5H_5)_2$ and $Mn(C_5H_5)_2$. This is partly due to the lowering of the averaged 3d levels in the latter two compounds. However, the major reason is attributed to the strong destabilization of the antibonding state. According to the multiple scattering Xα calculation by Weber *et al.*,[30,32] the energy separations between the a_1' and e_1' states are 4.98 eV for $Co(C_5H_5)_2$ and 4.57 eV for $Ni(C_5H_5)_2$.

Finally, the He*(2^3S) spectra of $Ru(C_5H_5)_2$ and $Os(C_5H_5)_2$ show that the $e_1''(\pi)$-derived band is much weaker than the nonbonding type $e_1'(\pi)$-derived band, where the intensity ratio $I(e_1'')/I(e_1')$ is only 0.34 in both cases. A similar suppression is also seen in the PIES of $Fe(C_5H_5)_2$, although the two bands overlap. These features indicate that the $e_1''(\pi)$ orbital has a compact electron distribution owing to the bonding d–π interactions, as expected from eqn. (1).

Branching ratio of ionic states in Penning ionization

In the above section we assumed that the Penning ionization rate depends essentially on the initial states in the collision systems. In this section we shall examine the branching ratio of the final ionic states in Penning ionization. For this purpose $Cr(C_5H_5)_2$ is a good example, because the multiplet structure is separated fairly well in both the UPS and the PIES. According to simple ligand field theory,[34] the intensity ratio of the e_2'-derived ionic states is given by $^4A_2' : {}^2A_2' : {}^2A_1' : {}^2E_1'' = 1.33 : 0.18 : 0.50 : 1$. Using these values and the relative photoionization cross sections [$k(a_1')/k(e_2') = 0.8$ for $Fe(C_5H_5)_2$],[5] Cauletti *et al.* predicted that the intensity ratio for band 1 to bands 2–4, is 0.54.[7] Their experimental ratio is 0.65 in the He I UPS, which is in agreement with our data (0.67 ± 0.1). They indicated that the predicted ratio is increased to 0.61 if the configuration interactions are taken into account. On the other hand, the corresponding intensity ratio is 1.30 ± 0.2 in the PIES. Since the Penning ionization cross section for the a_1' orbital is larger than that for the e_2' orbital, this means that the quartet $^4A_2'$ ionic state is markedly enhanced relative to the doublet states. The mechanism may be interpreted in terms of the spin-dependent entrance channels, *i.e.*, the singlet, triplet, and quintet channels. The latter channel such as He*(1s↑2s↑) + $Cr(C_5H_5)_2$ (e_2'↑↓↑a_1'↑) makes a dominant contribution on the statistical base and it leads only to the quartet $Cr(C_5H_5)_2^+$ ions because Penning ionization proceeds *via* the exchange process where a valence electron of $Cr(C_5H_5)_2$ fills the 1s hole of He* and the 2s electron is emitted. Owing to the spin restriction, the doublet species can not be produced in this channel. A similar phenomenon has been observed in the He*(2^3S)–$O_2(^3\Sigma_g^-)$ collision system, where the quartet states ($^4\Pi_u$ and $^4\Sigma_g^-$) are observed as prominent bands in the PIES but the doublet states ($^2\Pi_g$ and especially $^2\Pi_u$) are very weak.[19,35]

Conclusion

In this paper we presented the Penning ionization electron spectra (PIES) of gaseous metallocenes, $M(C_5H_5)_2$ (M = V, Cr, Mn, Fe, Co, Ni, Ru, and Os), using the He*(2^3S) metastable atoms. From systematic comparisons, our concluding remarks are as follows: (i) Penning ionization cross sections for the metal d-derived orbitals depend essentially on the collision geometry between He*(2^3S) and metallocenes, reflecting the spatial extent of the relevant wavefunctions. (ii) As a common feature of the 3d metallocenes, the metallic e_2'- and a_1'-derived bands are suppressed relative to the Cp π-derived bands in the PIES, which indicates that these metallic orbitals are localized inside the molecules owing to the essentially nonbonding character. In particular, the suppression is remarkable in the case of high-spin $Mn(C_5H_5)_2$ with substantially ionic bonding. On going from $Fe(C_5H_5)_2$ to $Ru(C_5H_5)_2$ and $Os(C_5H_5)_2$, the radial extent of the d orbitals increases, as expected. (iii) As for the metallic e_1'' orbitals in $Mn(C_5H_5)_2$, $Co(C_5H_5)_2$, $Ni(C_5H_5)_2$, they show rather diffuse electron distribution owing to strong antibonding d–π interactions. In contrast, the Cp π-derived e_1'' orbitals have compact electron distribution due to the bonding d–π interactions, which is clearly seen in the cases of $Ru(C_5H_5)_2$ and $Os(C_5H_5)_2$.

Acknowledgements

We would like to thank Prof. Y. Harada at Seitoku University for helpful discussion. Also we thank Dr. R. Suzuki, Mr. K. Yoshino and Ms. Y. Tanaka for their help with the experiments.

References

1 See, *e.g.*, E. I. Solomon and A. B. P. Lever, eds. *Inorganic Electronic Structure and Spectroscopy*, John Wiley and Sons, New York, 1999.
2 A. Haaland, *Acc. Chem. Res.*, 1979, **12**, 415 and references therein.
3 J. W. Lauher and R. Hoffmann, *J. Am. Chem. Soc.*, 1976, **98**, 1729.
4 J. W. Rabalais, L. O. Werme, T. T. Bergmark, L. Karlsson, M. Hussain and K. Siegbahn, *J. Chem. Phys.*, 1972, **57**, 1185.
5 S. Evans, M. L. H. Green, B. Jewitt, A. F. Orchard and D. F. Pygall, *J. Chem. Soc., Faraday Trans. 2*, 1972, **68**, 1847.
6 S. Evans, M. L. H. Green, B. Jewitt, G. H. King and A. F. Orchard, *J. Chem. Soc., Faraday Trans. 2*, 1974, **70**, 356.
7 C. Cauletti, J. C. Green, M. R. Kelly, P. Powell, J. Van Tilborg, J. Robbins and J. Smart, *J. Electron Spectrosc. Relat. Phenom.*, 1980, **19**, 327.
8 M. M. Rohmer and A. Veillard, *Chem. Phys.*, 1975, **11**, 349.
9 P. S. Bagus, U. I. Walgren and J. Almlof, *J. Chem. Phys.*, 1976, **64**, 2324.
10 K. D. Warren, *Struct. Bonding (Berlin)*, 1976, **27**, 45.
11 H. Hotop and A. Niehaus, *Z. Phys.*, 1969, **228**, 68.
12 K. Ohno, H. Mutoh and Y. Harada, *J. Am. Chem. Soc.*, 1983, **105**, 4555.
13 T. Munakata, Y. Harada, K. Ohno and K. Kuchitsu, *Chem. Phys. Lett.*, 1981, **84**, 6.

14 M. Aoyama, S. Masuda, K. Ohno, Y. Harada, C. Y. Mok, H. H. Huang and S. Y. Lee, *J. Phys. Chem.*, 1989, **93**, 1800.
15 Y. Harada, H. Mutoh and K. Ohno, *J. Chem. Phys.*, 1983, **79**, 3251.
16 S. Masuda and Y. Harada, *J. Chem. Phys.*, 1992, **96**, 2469.
17 S. Masuda and Y. Harada, *J. Am. Chem. Soc.*, 1990, **112**, 6445.
18 H. Tanaka, H. Yamakado and K. Ohno, *J. Electron Spectrosc. Relat. Phenom.*, 1998, **88–89**, 149.
19 O. Leisin, H. Morgner and W. Müller, *Z. Phys. A.*, 1982, **304**, 23.
20 P. E. Siska, *Rev. Mod. Phys.*, 1993, **65**, 337.
21 A. J. Yencha, *Electron Spectroscopy: Theory, Techniques and Applications;*, C. R. Brundle and A. D. Baker, eds., Academic, London, 1984, vol. 5, p. 197.
22 J. C. A. Boeyenes, D. C. Levendis, M. I. Bruce and M. L. Williams, *J. Crystallogr. Spectrosc. Res.*, 1986, **16**, 519.
23 P. Seiler and J. D. Dunitz, *Acta Crystallogr., Sect. B*, 1980, **36**, 2946.
24 E. S. Shubina, N. V. Belkova and L. M. Epstein, *J. Organomet. Chem.*, 1997, **536–537**, 17.
25 G. Orlova and S. Scheiner, *Organometallics*, 1998, **17**, 4362.
26 F. A. Cotton, G. Wilkinson, C. A. Murillo and M. Bochmann, *Advanced Inorganic Chemistry*, 6th edn., John Wiley and Sons, New York, 1999.
27 J. E. Huheey, *Inorganic Chemistry*, 3rd edn., Harper and Row Publishers, New York, 1983.
28 N. Rösch and K. H. Johnson, *Chem. Phys. Lett.*, 1974, **24**, 179.
29 E. J. Baerends and P. Ros, *Chem. Phys. Lett.*, 1973, **23**, 391.
30 J. Weber, A. Goursot, E. Pénigault, J. H. Ammeter and J. Bachmann, *J. Am. Chem. Soc.*, 1981, **104**, 1491.
31 C. Famiglietti and E. Baerends, *J. Chem. Phys.*, 1981, **62**, 407.
32 A. Goursot, E. Pénigault and J. Weber, *Nouv. J. Chim.*, 1979, **3**, 675.
33 C. Daul, H. U. Güdel and J. Weber, *J. Chem. Phys.*, 1993, **98**, 4023.
34 P. A. Cox, S. Evans and A. F. Orchard, *Chem. Phys. Lett.*, 1972, **13**, 386.
35 H. Hotop, E. Kolb and J. Lorenzen, *J. Electron Spectrosc. Relat. Phenom.*, 1979, **16**, 213.